Molecular-dynamics study of the synthesis and characterization of a fully dense, three-dimensional nanocrystalline material

S. R. Phillpot[a] and D. Wolf
Materials Science Division, Argonne National Laboratory, Argonne, Illinois 60439

H. Gleiter
Kernforschungszentrum Karlsruhe, 76021 Karlsruhe, Germany

(Received 22 February 1995; accepted for publication 5 April 1995)

A molecular-dynamics simulation method is described that permits space-filling, fully dense three-dimensional nanocrystalline materials to be grown by crystallization from the melt. The method is illustrated by computer synthesis of an eight-grain polycrystal of Cu with a grain size of 43 Å. At the beginning of the simulation, eight small pre-oriented single-crystal seeds are embedded in the melt which is subsequently cooled below the melting point to enable crystal growth under an applied external pressure. The fully relaxed nanocrystalline material contains large perfect-crystal regions separated by well-defined grain boundaries, most of which have approximately the same width and energy. In spite of the rather small number of grains in the simulation cell, the thermal expansion of the material is practically isotropic, and almost identical to that of the perfect crystal. The elastic moduli are also almost isotropic and are somewhat lower than in the coarse-grained material. The material exhibits a low-temperature anomaly in the specific heat. © *1995 American Institute of Physics.*

I. INTRODUCTION

The nature of grain boundaries (GBs) in nanocrystalline materials (NCMs) has been the subject of extensive discussion ever since the first ultrafine-grained polycrystals were synthesized a decade ago by consolidation of small clusters formed via gas condensation.[1,2] At issue is the question as to whether a novel, "frozen-gas"-like state of matter exists in polycrystalline materials with a grain size typically below 10 nm,[3,4] or whether the structure and properties of NCMs can be extrapolated from those of coarse-grained polycrystals. The concept that a novel state of matter may exist in extremely constrained, small-grained polycrystalline materials appears plausible considering that up to 50% of the atoms in such a material may be situated in the highly defected environments provided by the grain boundaries and grain junctions; such structural environments are not found in glasses (with short-range order) or crystals (with long-range order).

In spite of much experimental work on the structure and properties of nanocrystalline materials performed to date, a structural model consistent with the observations and one that permits some of the anomalous properties of these materials to be predicted, has not evolved. On the one hand, some recent observations involving Raman spectroscopy,[5] atomic-resolution transmission electron microscopy (TEM) combined with image simulations[6] and x-ray diffraction[7] indicate that the atomic structures of GBs in NCMs are, in fact, rather similar to those determined for coarse-grained polycrystalline or bicrystalline materials. On the other hand, observations involving Mössbauer spectroscopy,[8] conventional[9] and atomic-resolution TEM,[10] and x-ray diffraction[9,11] suggest the presence of nonequilibrium GBs in NCMs with structures and properties that differ significantly from those of coarse-grained materials. At present, it appears that without additional information coming, for example, from computer simulations, experimental investigations alone may not be capable of deriving a comprehensive structural model for these materials.

A situation similar to the one described existed until almost 30 years ago in the discussion about the atomic structure of GBs in coarse-grained polycrystals. Since then, extensive work involving atomic-level computer simulations combined with atomic-resolution experiments on bicrystalline GBs has shown that the additional information needed to develop a structural model can uniquely be extracted from such simulations. The most important features in the atomic structures of bicrystalline GBs thus exposed, which, in our view, may also be relevant in NCMs, may be summarized as follows:

(a) Rigid-body translations parallel to the GBs represent an important relaxation mechanism in minimizing the GB energy. One can expect that the severe geometrical constraints present in nanometer-sized polycrystals will prevent these translations from being optimized simultaneously for all the different GBs in the system and, therefore, will result in higher GB energies.

(b) Due to the destruction of the perfect-crystal stacking at the GBs, virtually all bicrystalline GBs show a volume expansion normal to the GB which is approximately proportional to the GB energy.[12] Experimental evidence suggests that when the rigid-body translations parallel to the GBs are not optimized, a larger volume expansion is needed to accommodate the misfit.[13]

(c) Like free surfaces, GBs tend to choose a structure which minimizes the number of broken bonds per unit GB area, i.e., to maintain as much as possible the perfect-crystal coordination even at the interface. The GB energy therefore correlates well with the number of broken bonds per unit GB area.[14] Another manifestation of this "broken-bond" model

[a]Electronic mail: simon_phillpot@qmgate.anl.gov

 0021-8979/95/78(2)/847/15/$6.00

is the strong localization of misfit seen commonly in high-resolution electron micrographs of all types of interfaces and materials.

(d) The radial distribution function, which in a disordered material is broadened even at zero temperature, gives the most detailed information on the atomic structure of the GBs.[15] The areas under the peaks can be related directly to the number of broken bonds at the GBs.

Any attempt to relate the structure and properties of GBs in a polycrystal to those of corresponding bicrystalline GBs, and hence to connect with the large body of knowledge that has been accumulated on the structure and properties of GBs in bicrystals, is extremely difficult as it requires three types of geometrical averages to be performed when producing the polycrystal. These averages arise from the microstructural (purely geometrical) constraints present in a polycrystal; they involve (a) the five macroscopic degrees of freedom that each individual GB contributes to the total number of degrees of freedom of the polycrystal, (b) the various grain shapes and (c) the distribution of grain sizes invariably present in polycrystals. Moreover, the task of assembling at the atomic level a space-filling polycrystal with a microstructure that is consistent with these types of averages while still containing crystallographically well-defined GBs is highly nontrivial.

Two types of theoretical studies of polycrystals have been performed in the past. In one, microstructural (or mesoscopic) in nature, an atomic-level description of the GBs is avoided by focusing on the three types of microstructural averaging.[16] In the other, two-dimensional polycrystals were constructed on usually triangular lattices, and atomistic simulations were used to determine relatively simple properties of the one-dimensional GBs in such a system.[17] Neither of these approaches connects directly with the atomic-level understanding that has been obtained for bicrystalline GBs.

By shifting the focus from the microstructure of the polycrystal to the atomic structure of the GBs, in this article we hope to address, as directly as possible, the relationship between the highly constrained GBs in nanocrystalline materials and the unconstrained GBs in bicrystals. Our main goal is to develop a molecular-dynamics (MD) simulation method to grow space-filling, fully dense three-dimensional polycrystals by crystallization from the melt and then to characterize them fully. To ensure a fully relaxed structure, the NCM will be annealed by heating to approximately half the melting temperature and then cooling back to zero temperature under zero external stress. This approach focuses on a description of the structure and properties of "relaxed", fully dense NCMs, i.e., irrespective of the kinetic processes that are, in practice, required to synthesize a fully dense NCM, we aim for a material that is free of pores and one that has been annealed such that the GBs are in some sort of a "relaxed ground state." Following the synthesis of such a somewhat idealized NCM, simulations can be used to determine its properties and to elucidate their connection with the underlying atomic structure of the GBs and grain junctions.

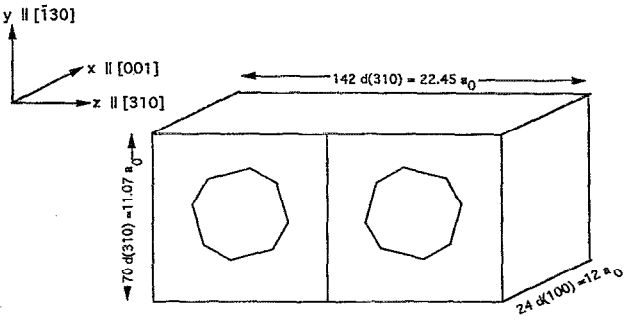

FIG. 1. Schematic of the $3d$ periodic simulation cell for the synthesis of the bicrystal, indicating the crystallographic orientation of the seeds and the dimensions of the simulation cell.

II. MOLECULAR-DYNAMICS SIMULATION OF THE GROWTH OF A Σ5 BICRYSTAL

Before simulating the synthesis of an actual polycrystal, we describe the molecular-dynamics (MD) synthesis of a bicrystal with a well-known zero-temperature structure. The purpose of this preliminary study is twofold. First, it allows suitable synthesis conditions (temperature, pressure, size and shape of the crystalline seeds) for crystal growth to be identified, which can subsequently be used for the synthesis of a polycrystal. Second, by comparing the GB structure thus obtained with the well-known zero-temperature structure of the same GB determined via iterative energy-minimization ("lattice-statics") simulation, the quality of the MD-grown bicrystal can be assessed.

The basic idea is to insert two small, pre-oriented crystalline seeds into the melt, cool the system below the melting point and apply external pressure to initiate crystal growth. The GB to be grown is the well-known Σ5 symmetrical tilt grain boundary (STGB) on the (310) plane of Cu. This GB may be thought of as having been generated by a tilt misorientation about [001] by the angle of $\psi=36.87°$. The three-dimensionally ($3d$) periodic simulation cell containing two small seeds with such a misorientation embedded in the melt is shown in Fig. 1. Because of the periodicity in the z direction in Fig. 1 (normal to the $x-y$ plane, in which the seeds are misoriented), *two* GBs will be formed during the simulation; their mutual separations are determined by the lengths in z of each of the two halves of the simulation cell. The latter were chosen of the order of 12 a_0 (where a_0 denotes the zero-temperature lattice parameter) to ensure a negligibly weak interaction between the GBs. Because of the periodicity in the $x-y$ plane (in which there is no misorientation across the cell borders), the GBs thus grown will be infinitely extended. Since our subsequent polycrystal simulation is most conveniently performed on a cubic simulation cell, the lengths of the simulation cell in the x and y directions were chosen to be of similar magnitude.

Unfortunately, choosing two exactly cubic boxes in Fig. 1 will not permit the growth of two identical (310) STGBs. Consequently, in order to ensure that the two GBs to be grown can be as nearly identical as possible, particularly with respect to their rigid-body translations parallel to the GBs, special care has to be taken in (a) positioning the seeds

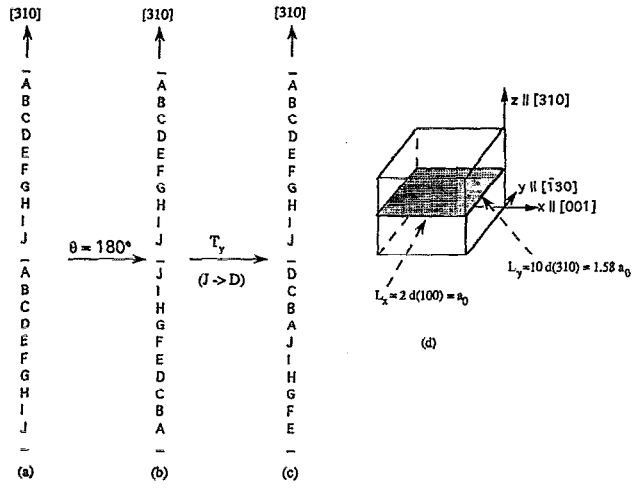

FIG. 2. Generation of the STGB on the (310) plane as a 180° twist boundary (Ref. 18). (a) Two perfect-crystal stacks of (310) planes. As illustrated in (b), twisting the bottom half with respect to the top half by 180° results in the inversion of the stacking sequence in the bottom half. A subsequent rigid-body translation parallel to the [1̄30] direction in the plane of the GB leads to the lowest-energy translational configuration illustrated in (c). (d) Schematic of the $3d$ periodic planar unit cell for the (310) STGB, showing the unit-cell dimensions.

correctly within the simulation cell and (b) fixing the precise lengths of each of the two halves of the simulation cell in the z direction. To illustrate these points it is necessary to consider in some detail the geometry and optimum rigid-body translation of the GB which we hope to grow (see Fig. 2).

The planar unit-cell geometry of the (310) STGB, in particular its optimum rigid-body translation, is most conveniently seen by thinking of this GB as having been generated by a 180° twist boundary about the (310) GB-plane normal.[18] Figure 2(a) shows the 10-plane ...|*ABCDEFGHIJ*|... stacking period P of (310) planes in the perfect crystal [i.e., $P(310)=10$]. Starting with the two perfect-crystal stacks of planes in (a), the STGB configuration on the (310) plane is readily obtained by a 180° twist rotation of, say, the bottom stack with respect to the top stack, leading to the stacking inversion illustrated in Fig. 2(b). A rigid-body translation parallel to the GB (such that $J\rightarrow D$, $I\rightarrow C$, etc.) eliminates the energetically unfavorable mirror-plane configuration in (b) in which two J planes face each other directly across the GB. This leads to the minimum-energy translational configuration sketched in (c), which was determined from lattice-statics simulations.

The rectangular *primitive* planar unit-cell dimensions of this GB, L_x and L_y [see Fig. 2(d)], are identical to those of the perfect-crystal (310) planes in (a) because the stacking inversion does not affect the planar periodicity.[18] Given the interplanar spacings in the face-centered-cubic (fcc) lattice, $d(310)=0.158\ a_0$ and $d(100)=0.5\ a_0$, and the two-plane stacking sequence of (001) planes $P(100)=2$, L_x and L_y are given by [see Fig. 2(d)] $L_x=2d(100)=a_0$ and $L_y=10d(310)=1.58\ a_0$, with an area $A(310)=1.58\ a_0^2$. The periodicity of this primitive, perfect crystal-like *planar* repeat unit cell is identical to that of the $3d$ periodic $\Sigma 5$ coincident-site-lattice (CSL) unit cell projected onto the GB plane.

For the two GBs in the MD-grown bicrystal to be strictly periodic in the $x-y$ plane (see Fig. 1), the lengths of the simulation-cell edges must be multiples of L_x and L_y. Also, to ensure that the rigid-body translational states of the two GBs in the periodically repeated z direction are identical, the number of (310) planes in the z direction must be a multiple of the (310) stacking period *plus one plane*. These considerations have led us to choose a simulation cell in Fig. 1 consisting of two nearly cubic, right-angled boxes with sides of length $D_x=24d(100)=12\ a_0$, $D_y=70d(310)=11.07\ a_0$, and $D_z=71d(310)=11.23\ a_0$. Given the atomic volume in the fcc lattice of $0.25\ a_0^3$, each half of the MD simulation cell thus formed contains $4D_xD_yD_z=5964$ atoms, for a total of 11928 atoms in the entire system.

The crystalline seeds were chosen to represent truncated octahedra with {111} and {100} faces, the two lowest-energy surfaces in the fcc structures. Each seed contains 586 atoms (or 9.8% of the total number of atoms in each half of the system). The faces of the seeds are large enough to ensure that the surfaces of the truncated octahedra are crystallographically clearly identifiable. Each pair of parallel {100} faces is separated by $6\ a_0$; the distance between each of the seeds and the simulation-cell edges is 3, 2.53, and 2.61 a_0 in the x, y, and z directions, respectively, i.e., the separation between seeds in the x, y, and z directions is 6, 5.07, 5.23 a_0, respectively (see Fig. 1).

The initial simulation-cell geometry sketched in Fig. 1 is generated by setting up a (310) STGB with the simulation-cell dimensions and optimal rigid-body translation already described. This system is then melted; however, to provide nuclei for the subsequent growth of the bicrystal, the atoms in the seeds were held fixed. This results in well-matched crystal–liquid interfaces surrounding the seeds, from which the bicrystal growth can then proceed. To ensure that the system thus prepared has lost all its memory of the crystalline state, the system was kept at a temperature well above the melting temperature for a long period of time (however, with the seed atoms fixed) during which extensive diffusion occurred in the liquid. An alternate method of achieving the same initial state (of the seeds surrounded by liquid) would be to start from an entirely liquid simulation cell, and to replace a spherical region of liquid atoms with a properly oriented, truncated octahedral seed embedded in a shell of liquid atoms. This method, used in the preparation of the polycrystalline simulation cell, works equally well (see Sec. III).

Since we are not interested in the properties of any specific material, the Lennard-Jones (LJ) potential was used to describe the interatomic interactions. In the LJ potential, the interaction energy $v(r_{ij})$ between atoms i and j, separated by a distance r_{ij}, is

$$v(r_{ij})=4\epsilon\left[\left(\frac{\sigma}{r_{ij}}\right)^{12}-\left(\frac{\sigma}{r_{ij}}\right)^{6}\right]. \tag{1}$$

The energy and length scales in this potential ($\epsilon=0.167$ eV, $\sigma=2.315$ Å) were fitted to the melting point, $T_m=1356$ K, and zero-temperature lattice parameter, $a_0=3.616$ Å, of Cu, with a cohesive energy, $E_{id}=-1.0378$ eV/atom. The potential is shifted and smoothly cut off after the fourth-neighbor

shell.[19] Extensive comparisons with physically better justified many-body potentials have shown that this simple potential represents fcc metals remarkably well, particularly the energies of GBs,[20] and the elastic[21,22] and thermoelastic properties[23] of multilayers composed of GBs. This similarity between the two types of potentials is due to the fact that most interfacial phenomena are dominated by the short-range repulsions between the atoms (which are central force in both types). We are, therefore, confident that the physical behavior of the LJ model bicrystal and polycrystal described here is very similar to what would be obtained by means of a computationally more costly (typically by a factor of two) many-body potential.

As a benchmark against which to compare the MD-grown bicrystal, we calculated the equilibrium zero-temperature structure and energy of the (310) STGB by lattice-statics simulation. The optimum (i.e., lowest-energy) translational state was that given in Fig. 2(c). The GB energy γ and the related volume expansion per unit GB area δV (a volume per unit area, and usually given in units of the lattice parameter) thus obtained are $\gamma=860$ erg/cm^2 and $\delta V=0.155\ a_0$.

The MD simulations were performed using both constant-strain and constant-stress codes incorporating a link-cell list.[19] Throughout, the time step was 6×10^{-15}, for which energy was found to be conserved to 1 part in 10^4, with no systematic energy drift. In the constant-temperature simulations, a thermostat was applied by velocity rescaling at every time step.

As already mentioned, the initial simulation geometry sketched in Fig. 1 was prepared by heating the carefully chosen $T=0$ K bicrystalline system to 1400 K, approximately 200 K above the melting temperature for this potential ($T_m\approx1200$ K) with the seed atoms fixed. After equilibrium, the energy distribution of the nonseed atoms in the system was indistinguishable from that of a bulk liquid at the same temperature. Starting from this initial geometry (liquid plus two pre-oriented seeds), the MD simulation of the growth of the bicrystal was performed in the following three steps.

(1) The system was suddenly (i.e., in one time step) cooled down from 1400 to 1075 K (i.e., below T_m) and a compressive external pressure was applied. The latter was imposed by isotropically reducing the volume of the simulation cell so that the average lattice parameters in the x, y, and z directions were equal to the lattice parameter of the perfect crystal at 1075 K. With the seed atoms fixed, the system was then allowed to evolve at constant volume. The structure of the system was stored every 3 ps for subsequent analysis. The energy was calculated for each of the saved structures and, as described in more detail below, the atomic structure was analyzed by examining the nearest-neighbor (nn) coordination of the atoms. After ~87 ps of simulation time the energy of the system stopped decreasing and the simulation was halted shortly thereafter.

(2) The system resulting from step (1) was suddenly cooled consecutively to 900, 700, and 500 K at 6 ps (=1000 time steps) intervals at the lattice parameters of the ideal crystal at that temperature. Next, the temperature was reduced consecutively to 300, 200, 100, and 1 K at 6 ps intervals. At each of these latter temperatures the size of the simulation cell was allowed to adjust to give zero external stress while the seed atoms were allowed to move.

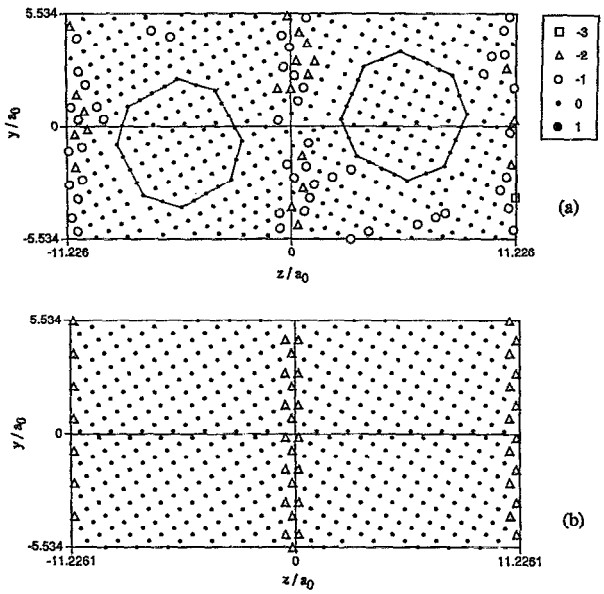

FIG. 3. Positions and nn miscoordinations of atoms in a slice of thickness 0.5 a_0 centered about $x=0$ in (a) the MD-grown bicrystal, and (b) the 0 K bicrystal generated by lattice-statics calculation. The [310] direction is parallel to the z axis, while the x direction is oriented along [001]. Here and in subsequent similar figures the different symbols denote different atomic miscoordinations (between -3 and $+1$ as indicated in the legend). The atoms originally in the crystalline seeds are enclosed by the solid lines.

(3) The structure obtained at 1 K was relaxed via lattice-statics simulation at zero stress with the seed atoms allowed to move. This yielded the zero-temperature structure of the bicrystal in which the forces on all the atoms and the stresses on the simulation cell vanish.

To illustrate the final atomic structure thus obtained, the positions of the atoms in slices in the $y-z$ plane of thickness 0.5 a_0 (the spacing of {100} planes) about the center of the simulation cell are shown in Fig. 3(a). For comparison, Fig. 3(b) shows the $T=0$ K equilibrium structure of the same bicrystalline system, as determined by lattice-statics simulation. In these figures, and in subsequent similar figures for the polycrystal, the atoms are distinguished by their nn miscoordination, M_i, (i.e., the deviation of the number of nns of atom i from the 12 nns in the perfect crystal). For example, $M_i=+1$ (-1) if atom i has 13 (11) nearest neighbors. (Two atoms are considered to be nns if their separation is less than, or equal to, half the distance between the perfect-crystal nearest and second-nearest neighbors, scaled to take account of the actual lattice parameter of the simulated system.) Figure 3(b) shows that in the $T=0$ K bicrystal, large perfect-crystal regions are separated by well-defined regions of miscoordinated atoms only about three atomic layers thick. By contrast, the miscoordinated regions in the MD-grown bicrystal are somewhat wider [~4–5 (310) planes]; also, the as-grown material exhibits growth defects in the perfect-crystal regions and the GB structures are not as well ordered. To investigate whether this absence of strict CSL periodicity

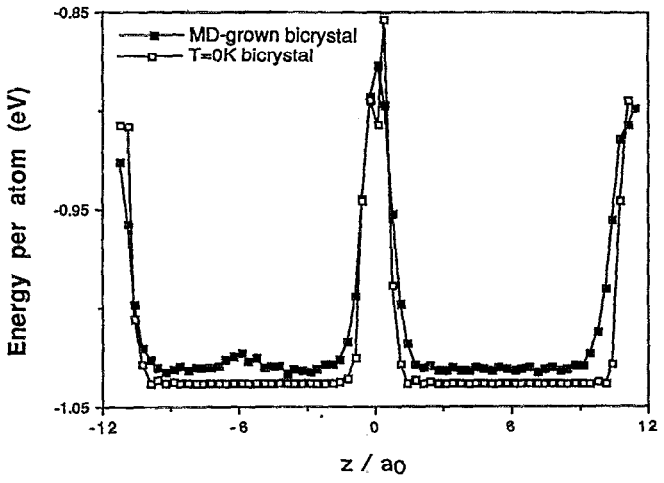

FIG. 4. The mean energy per atom as a function of the z coordinate (see Fig. 1) in slices of thickness 0.33 a_0 for the MD-grown bicrystal and for the $T=0$ K bicrystal. The close matching of the energy profiles indicates the high-quality of the MD-grown bicrystal.

parallel to the GBs is a kinetic effect associated with our synthesis conditions, or whether it is intrinsic to the high-temperature structure of the GBs and was frozen in by rapidly quenching to zero temperature, we annealed the bicrystal by repeatedly heating to approximately half the melting temperature and recooling to zero temperature. We found that the nonperiodic structure remains stable on the MD time scale of these anneals, strongly suggesting that the nonperiodicity is an inherent part of the high-temperature structure.

To quantify the structural quality of the MD-grown bicrystal, we use the following four measures: the nn miscoordination per unit GB area C, the GB width δ_{GB}, the GB energy γ, and the GB volume expansion per unit area δV. The miscoordination per unit area is defined as [14,20]

$$C=\frac{1}{A}\sum_{i=1}^{N}|M_i-12|, \tag{2}$$

where A is the total GB area and N the total number of atoms in the system. For a perfect crystal, $C=0$. The $T=0$ K bicrystal is much better coordinated (with $C=6.3\ a_0^{-2}$) than the MD-grown bicrystal (with $C=9.5\ a_0^{-2}$). While much of the extra miscoordination comes from the less well-ordered GB regions [compare Figs. 3(a) and 3(b)], part of it is attributable to the growth defects in the bulk perfect-crystal regions.

Figure 4 compares the mean energy per atom in slices of thickness 0.33 a_0 as a function of z position through both the MD-grown bicrystal and the $T=0$ K bicrystal. It is clear from Fig. 4 that the distributions of energies in the GB regions are remarkably similar for the two bicrystals, but that they decay to somewhat different bulk values. To quantify this observation, we define somewhat arbitrarily the GB width, δ_{GB}, as the width of the region surrounding the interface with energy greater than -1.0 eV (the perfect-crystal cohesive energy being $E_{id}=-1.0378$ eV). From Fig. 4 we find $\delta_{GB}=1.6\ a_0$ for the $T=0$ K bicrystal and $\delta_{GB}=2.2\ a_0$ for the MD-grown bicrystal. The energy in the center of the bulk-like regions E_b of the MD-grown bicrystal is somewhat higher ($E_b=-1.012$ eV) than in the perfect crystal, indicative of the presence of growth defects [see, for example, Fig. 3(a)].

To further compare the quality of the two bicrystals, the GB energy γ defined as

$$\gamma=(E-E_{id})N/A \tag{3}$$

was calculated. Here E is the average energy per atom in the bicrystal and N is the total number of atoms in the system. Using Eq. (3), we obtain a value of $\gamma=1400$ erg/cm^2 for each of the two GBs in the MD-grown bicrystal (compared to 860 erg/cm^2 determined for the $T=0$ K bicrystal). However, because growth defects result in the energy of the bulk-like regions being somewhat higher than in the perfect crystal, a better measure of the mean GB energy is obtained by replacing E_{id} in Eq. (3) by the previously determined value of E_b. The GB energy then obtained decreases to 1100 erg/cm^2, which is only 28% higher than the energy of the $T=0$ K bicrystal. Finally, the related excess volumes determined for each of the two GBs in the MD-grown bicrystal (from the change in length of the simulation cell normal to the interface) is 0.157 a_0, which is almost identical to the bicrystalline value of 0.155 a_0.

In conclusion, this preliminary study demonstrates that it is, indeed, possible to define an appropriate set of growth conditions that enable the MD synthesis of a bicrystal of reasonably high quality from small, pre-oriented crystalline seeds inserted into the melt. In the next section this "growth recipe" will be used to synthesize a nanocrystalline material.

III. SYNTHESIS AND CHARACTERIZATION OF A NANOCRYSTALLINE MATERIAL

The size of the simulation cell used for the growth of a NCM was chosen in the following way. For the system to be isotropic and the grain-size distribution to be realistic, it is desirable to include as many grains as possible in the simulation cell. In addition, the average grain size should be of nanometer dimensions (typically 5–10 nm) such that a connection with experimentally produced NCMs can be made. To keep the size of the simulated system within reasonable limits, in this first study of its kind we have not attempted to produce a realistic (usually log-normal) grain-size distribution. As a suitable compromise between the desired grain size and the number of grains, on the one hand, and computational limitations, on the other, we have chosen a system containing eight grains arranged on a simple cubic lattice (see Fig. 5), producing a total of 24 different GBs. The initial average distance between the eight crystalline seeds fixes the average grain size to 12 a_0=43.4 Å, i.e., near the lower end of the experimental range; this system contains 55296 atoms. In spite of this small number of grains and GBs, the material thus obtained is surprisingly isotropic.

A. Initial simulation geometry

To set up the initial cubic simulation cell sketched in Fig. 5, the eight octants, each containing a pre-oriented crystalline seed surrounded by liquid, were prepared in the following three steps, using the bicrystal simulations as starting point.

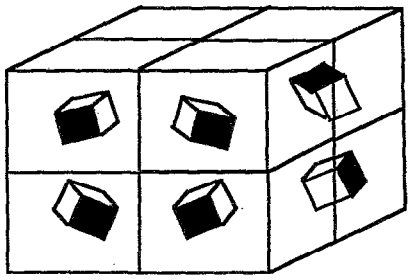

FIG. 5. Schematic of the simulation cell used for the MD growth of an eight-grain polycrystal showing the oriented seeds positioned near the centers of the octants of the cubic cell. In this perspective, only six of the eight seeds are sketched. For simplicity, the truncated octahedral seeds are shown as cubes.

(1) At an early time during the simulation of the *bicrystalline* system shown in Fig. 3(a), we have removed a sphere of radius $r=4.156\ a_0$ that contains 1048 atoms, including the 586-atom truncated-octahedral seeds onto which very little crystal had grown. Since this sphere was removed from a system at $T=1075$ K, with a lattice parameter appropriate for that temperature ($1.0139\ a_0$), all the atom positions were scaled by 1/1.0139 to give a $T=0$ K sphere of radius $4\ a_0$.

(2) The extracted sphere was rotated to an appropriate orientation and then placed near the centers of eight identical, completely melted cubes of side $12\ a_0$ (each containing 6912 atoms), with the subsequent removal of a sphere containing an equal number of liquid atoms. To ensure more or less random initial rigid-body translations at the GBs, the centers of the seeds were displaced randomly from the centers of the cubes by a small amount ($<0.5\ a_0$).

(3) These eight cubes were then assembled to form the cubic simulation cell sketched in Fig. 5, with sides of length $24\ a_0$ and containing a total of 55296 atoms.

Although completely random orientations of the seeds would most likely result in a more isotropic NCM, in order to be able to compare the polycrystal with a few well-known "special" bicrystalline GBs, the seeds were inserted with well-defined, not completely random orientations. The $3d$ periodic simulation cell in Fig. 5 contains a total of 24 GBs, including 12 pairs of GBs with the same misorientation. By contrast with the carefully chosen initial rigid-body translations in setting up the bicrystal simulation cell in Fig. 1, the random translations chosen here result in different atomic structures of the two GBs in each of the 12 pairs, in spite of their identical misorientations. Figures 6(a)–6(c) illustrate schematically how four of the 12 misorientations were fixed by choosing certain crystallographic orientations of the eight seeds.

(a) So as to enable a comparison with the (310) bicrystal studied in the previous section, the seeds in the two upper octants in Fig. 6(a) were oriented with the [310] and [001] directions parallel to the x and z directions, respectively. The GB thus formed on the $y-z$ plane is the (310) STGB.

(b) The seeds in the two lower octants in Fig. 6(a) were oriented such that the [111] directions are parallel to the x axis. This orientation is of particular interest since, at the optimum translational state of the (111) STGB thus formed,

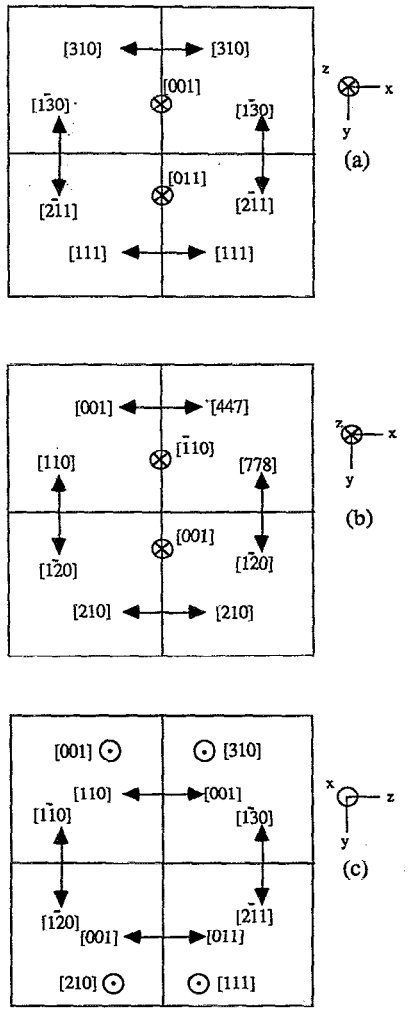

FIG. 6. Schematic of the eight-grain polycrystal showing the crystallographic orientation of the seeds projected onto (a) the $x-y$ plane for $z>0$, (b) the $x-y$ plane for $z<0$, and (c) the $y-z$ plane for $x<0$. If the GBs were to grow parallel to the edges of the simulation cell, the eight grains would be delimited by 8 tilt boundaries and 16 general boundaries.

this so-called coherent fcc twin has an extremely low energy (1 erg/cm^2 for the LJ potential) because only the third-nns of the atoms at the GB are affected by the presence of the interface. However, as mentioned in the Introduction, a small rigid-body translation away from the optimum translation, as is likely the case in the constrained environment of NCMs, can lead to a very large increase in the GB energy,[18,20] up to 701 erg/cm^2 for the energetically least favorable translational state in the bicrystal.

(c) The seeds in the two upper octants in Fig. 6(b) were oriented with the [001] and [447] directions parallel to the x direction, thus generating an asymmetrical (001)(447) tilt boundary, with the [$\bar{1}$10] tilt axis parallel to the z direction.

(d) The seeds in the two lower octants in Fig. 6(b) were oriented with the [210] directions parallel to the x axis; the (210) STGB that can thus be formed is also well known from bicrystal studies at $T=0$ K.

Because of the $3d$ periodic border conditions, each of these four "special" misorientations is capable of producing

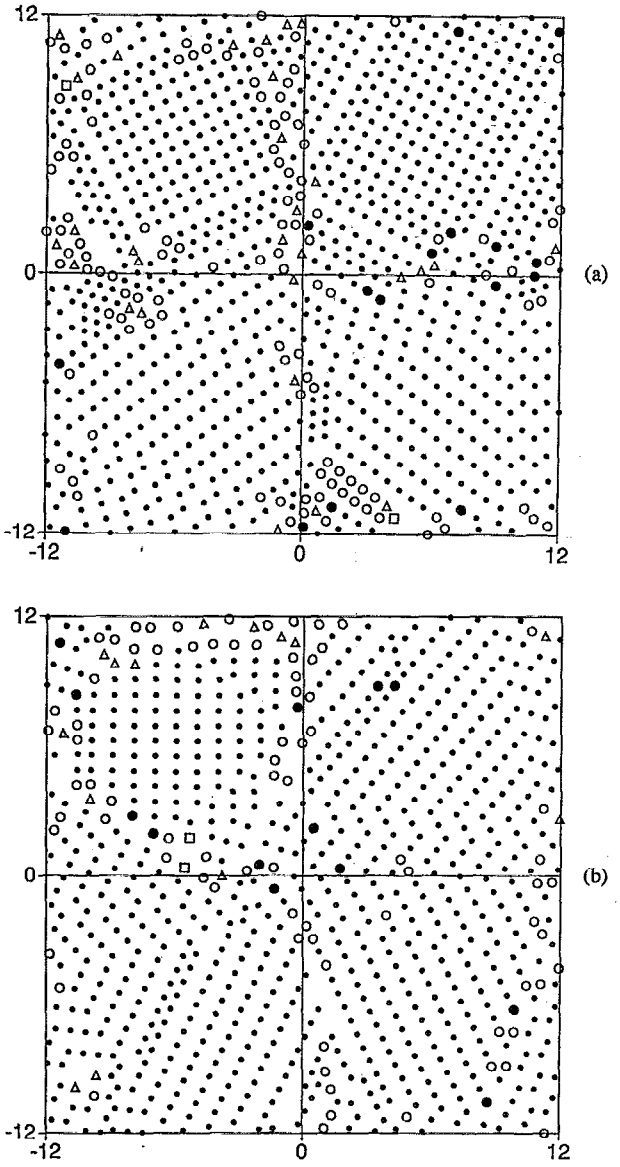

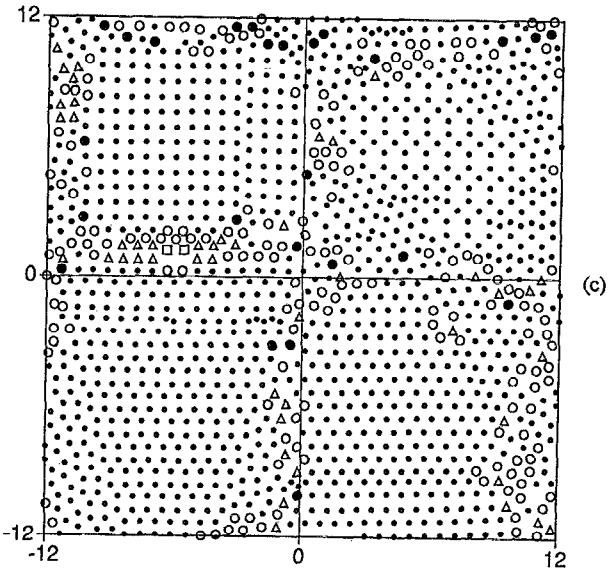

FIG. 7. Structural cross sections (a)–(c) are through the centers of the seeds in Figs. 6(a)–6(c). The thicknesses of the cross section of 0.4, 0.375, and 0.5 a_0, respectively, are chosen to most clearly show the interface structure. As in Fig. 3, the symbols denote different atomic miscoordinations.

two commensurate GBs with different rigid-body translations and, hence, atomic structures. As indicated in Figs. 6(a)–6(c), by necessity the remaining eight pairs of GBs are asymmetric tilt or twist (i.e., "general" or "random") GBs. Most of these are not even commensurate, by contrast with the four pairs already chosen; however, the $3d$ periodicity will force these GBs to be periodic on the length scale of the simulation cell.

B. Synthesis

Using the simulation-cell geometry described above, the polycrystal was grown under the same conditions as the bicrystal (see Sec. II), i.e., at a temperature of 1075 K and at the density of the perfect crystal at 1075 K. After ~66 ps of simulation time, the energy of the system stopped decreasing and the crystalline regions stopped growing (as indicated by the number of miscoordinated atoms ceasing to decrease). At this point, the temperature was reduced in a stepwise manner to 1 K (see Sec. II). For $T \leqslant 300$ K, the atoms in the seeds were allowed to move and the stresses on the system were relaxed by means of constant-(zero)-stress MD simulations. The final 1 K structure was subjected to a lattice-statics relaxation until the total energy, the atomic forces, and the stresses were suitably converged.

To ensure that the material thus obtained is reasonably stable, prior to the structural characterization to be described, the system was subjected to thermal cycling at zero external stress. This involved heating to 600 K ($\approx 0.5\ T_m$) in 100 K steps, with 12 ps at each temperature, followed by cooling back to 0 K in the same manner. The final structure was found to be virtually identical to the initial structure (i.e., the energy, simulation-cell dimensions, and the number of miscoordinated atoms remained essentially unchanged), demonstrating the stability of the polycrystal over this temperature range, at least on an MD time scale.

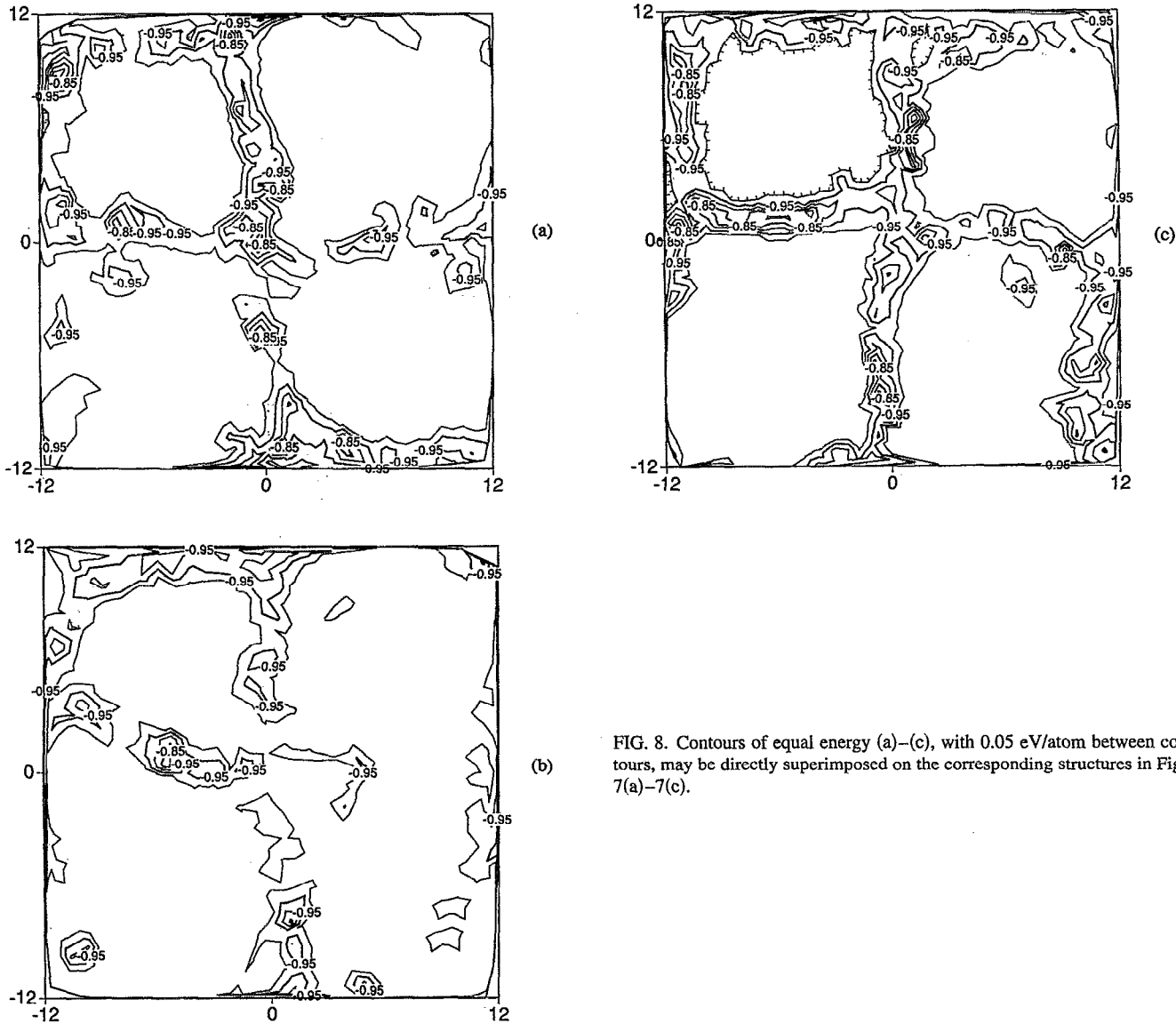

FIG. 8. Contours of equal energy (a)–(c), with 0.05 eV/atom between contours, may be directly superimposed on the corresponding structures in Figs. 7(a)–7(c).

C. Local structure, energy, and stress

Figures 7(a)–7(c) display the positions of the atoms in cross sections through the centers of the grains sketched schematically in Figs. 6(a)–6(c). As in Sec. II, the atoms are labeled in accordance with their nearest nn miscoordination. These structures clearly illustrate that the perfect-crystal seeds have acted as nucleation centers for the growth of extended regions of highly ordered material. The presence of fairly localized GBs can be seen in the form of chains of miscoordinated atoms approximately parallel to the edges of the simulation cell. As in the bicrystal, growth defects, such as point defects, clusters of point defects and dislocations, are found in the grain interiors. The related contours of equal energy in Figs. 8(a)–8(c) demonstrate that the higher-energy regions in the material are mostly localized in the relatively narrow GB regions.

We now examine the four pairs of "special" GBs grown from carefully preoriented seeds. Not surprisingly, in the severely constrained NCM, the rigid-body translations parallel to all the GBs cannot be optimized simultaneously, resulting in significantly increased energies of the lowest-energy bicrystalline GBs. For example, the energies of the two (111) "twins" in the lower half of Figs. 7(a) and 8(a) (one in the lower center of the figure and one, due to the $3d$ periodicity, across the lower vertical edges) are considerably higher (200 and 630 erg/cm^2, respectively) than in the bicrystal (1 erg/cm^2); this increase is due to the absence of a twinning plane in the NCM, as is clearly seen from Fig. 7(a).

Particularly striking is the large variation in the atomic structures along all the GBs in Fig. 7, which is also reflected in the energy contours in Fig. 8. To quantify this observation, the GB energies obtained from four nonoverlapping, square regions of size $3\ a_0 \times 3\ a_0$ extending $\pm 6\ a_0$ into the grains were determined for each of the two (111) STGBs. For the boundary in the bottom center in Figs. 7(a) and 8(a), "local" GB energies of 960, 420, 250, and 900 erg/cm^2 were thus obtained, giving the mean value of 630 erg/cm^2 mentioned above. It is interesting to note that two of these four seg-

ments have energies that are even higher than the energetically worst translational configuration of the related bicrystal (of 701 erg/cm^2);[18] it appears that this effect arises from the microstructural constraints imposed on the GB due to the presence of the other grains. By contrast, for the (111) STGB across the edge of the simulation cell, energies of 10, 280, 500, and 10 erg/cm^2 were determined, giving a mean of 200 erg/cm^2.

A similar analysis for the two STGBs on the (310) plane in the upper half of Figs. 7(a) and 8(a) gives "local" GB energies of 1090, 930, 1010, and 1030 erg/cm^2, with a mean value of 1020 erg/cm^2, for the GB in the center of the cell, and values of 770, 830, 670, and 950 erg/cm^2, with a mean value of 800 erg/cm^2, for the GB across the vertical edges. These energies are closer to the lowest bicrystalline value of 860 erg/cm^2 associated with the optimum rigid-body translation[20] than to that of the energetically worst translational configuration of 1750 erg/cm^2.

The energies of the two (001) (447) asymmetrical tilt boundaries in the polycrystal [of 810 and 790 erg/cm^2; see the upper octants in Fig. 6(b)] are only slightly higher than the optimum bicrystal value of 710 erg/cm^2.[20] By contrast, the energies of the polycrystalline (210) STGBs [of 520 and 350 erg/cm^2; see the lower octants in Fig. 6(b)] are considerably lower than the lowest value determined via lattice-statics simulation of the corresponding bicrystalline GB (910 erg/cm^2).[20] This large difference suggests the existence of relaxations (such as GB reconstruction) in MD-grown GBs that do not exist in bicrystals produced by lattice-statics relaxation. Indeed, simulations using the same LJ potential have shown that bulk-terminated high-energy twist GBs can reconstruct to lower-energy configurations by incorporation of vacancies into the GB region.[24] While such reconstructions are not accessible in lattice-statics simulations, it appears that the high atomic diffusion in the liquid can make such reconstructions accessible to GBs grown by MD.

A useful, although somewhat arbitrary measure of the GB width can be obtained from the excess-energy profile across the GB. In Fig. 9 the energy per atom across two sections of the (310) symmetric-tilt boundary in the lower center of Fig. 8(a) is compared with that of the related bicrystal. As in Sec. II (see Fig. 4), we define the width δ_{GB} as the region with energy greater than -1.0 eV/atom (with $E_{id}=-1.0378$ eV); this yields the values $\delta_{GB}\approx 2.8$ and ≈ 3.5 a_0, respectively, for the two NCM profiles and $\delta_{GB}\approx 1.6$ a_0 for the bicrystal.

In a "real-world" polycrystal it can be expected that nearly all GBs are "random" boundaries, with both tilt and twist components; the four pairs of "special" GBs examined are, therefore, not representative. The remaining eight pairs of GBs, including those shown in Figs. 7(c) and 8(c), are such boundaries; they exhibit two particularly striking features. First, their energies, varying between approximately 640 and 1040 erg/cm^2, with an average of 840 erg/cm^2, are rather similar. Second, their widths are rather uniform, typically about 2.5–3.5 a_0.

We finally examine the distribution in the stresses corresponding to the structures and energy profiles in Figs. 7 and 8. According to Figs. 10(a)–10(c), the stress varies significantly along the GBs and even across the grain interiors. In particular, in several GBs tensile and compressive regions coexist. By contrast, most of the grain interiors are slightly compressed; as discussed below, this effect gives rise to a densification of the perfect-crystal regions. The observations may be summarized as follows.

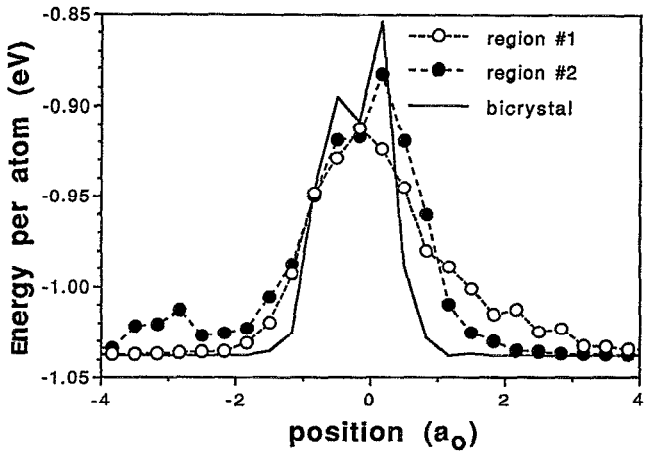

FIG. 9. Mean energy per atom as a function of the x coordinate in Fig. 6(a) for two different 3 $a_0\times 3$ a_0 sections of the (310) symmetric tilt boundary at the center of the upper half of Figs. 6(a), 7(a), and 8(a) crystallized from the melt compared with the energy profile for the same GB in a $T=0$ K bicrystal.

(a) In the severely constrained NCM, the rigid-body translations parallel to all the GBs cannot be optimized simultaneously, resulting in significantly increased energies of the lowest-energy bicrystalline GBs, as evidenced most strikingly by the (111) STGB. By contrast, GBs already with very high energies in the bicrystal have similar or even slightly lower energies in the NCM, suggesting that bicrystalline GBs that are already very disordered cannot be disordered further even under the severe microstructural constraints. Based on these effects, one can expect a much narrower distribution of the GB energies in the NCM than in bicrystals and a relatively uniform GB width.

(b) Another important difference from bicrystalline GBs is the virtually complete absence of strict structural periodicity parallel to the GBs in the NCM. The presence of such periodicities in bicrystalline GBs forms the basis of the description of high-angle GBs in terms of the CSL and, in the same spirit, in terms of polyhedral building blocks.[25,26] That neither of these concepts can be applied is seen clearly for all the GBs in Figs. 7 and 8. The effect is particularly noticeable for the (111) "twin" in which small regions of twin-like material coexist with heavily disordered regions. By contrast, the zero-temperature CSL-based structure of this GB has the extremely small ($\sqrt{2}/2$ $a_0\times\sqrt{2}/2$ a_0) rhombohedral periodic planar unit cell of the perfect-crystal (111) planes, which is clearly not obtained here.

The absence of strict periodicity parallel to the GBs may have two causes. First, while it is well-known that in a bicrystal at zero temperature various stable structures with different rigid-body translations may coexist, the severely constrained environment of the NCM forces the creation of additional, higher-energy translational states [as evident, for

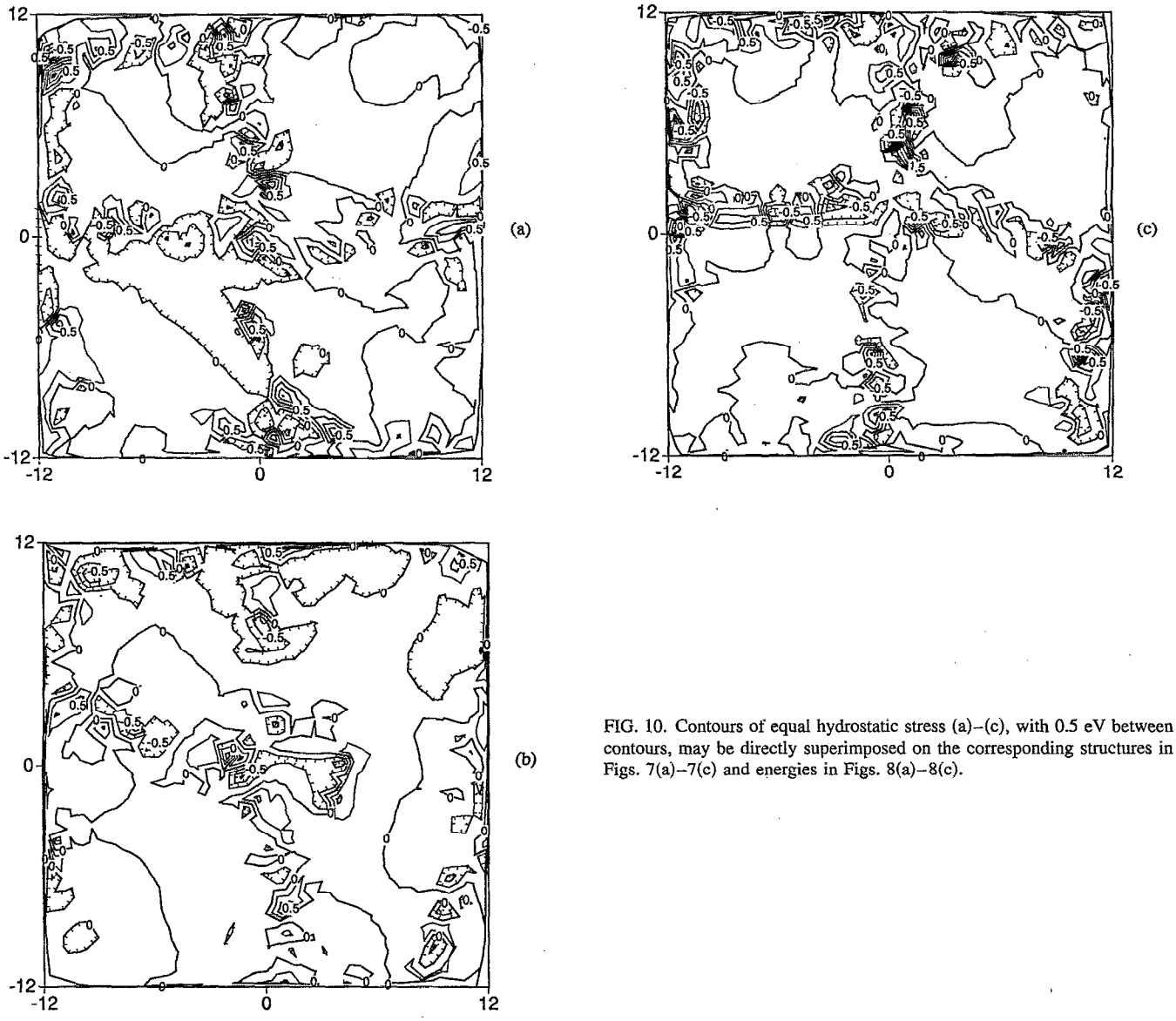

FIG. 10. Contours of equal hydrostatic stress (a)–(c), with 0.5 eV between contours, may be directly superimposed on the corresponding structures in Figs. 7(a)–7(c) and energies in Figs. 8(a)–8(c).

example, in the (111) "twin"], giving rise to the coexistence of many short GB segments with different translations. Second, our GB synthesis from the melt enables regions of configuration space to be sampled, which are not accessible at low temperatures (see also Sec. II).

As noted earlier, in contrast to the above observations, some high-resolution TEM experiments[6] have reported rather similar GB structures in NCMs and in coarse-grained materials. Whether this discrepancy is due to intrinsic effects associated with the very small grain size in our simulations, or due to relaxations introduced when preparing the thin microscopy samples or other experimental limitations, remains to be investigated.

D. Average structure and energy

The local type of information already mentioned is typically available only from simulations. Most experiments provide only system averages (such as the average density, the radial distribution function, the average number of broken nn bonds and the excess-energy density), thereby averaging over the local inhomogeneities due to the GBs and grain junctions. In the following we investigate such system averages.

Although our simulation cell was initially cubic, at the end of the simulation it is slightly noncubic, with mean lattice parameters in the x, y, and z directions (see Fig. 6) that are slightly larger than that of the perfect crystal [by 0.22 (0.91%), 0.23 (0.95%), and 0.16 a_0 (0.65%), respectively]. This slight anisotropy is due to the insufficient microstructural averaging in our material containing only a small number of grains and GBs. The slight zero-temperature expansion of the system indicates a lower density of the NCM (97.5% of that of the perfect crystal). If we assume that the entire excess volume is localized at the GBs and that all GBs are parallel to the faces of the simulation cell (see Figs. 7 and 8), an average GB excess volume per unit GB area, δV, of

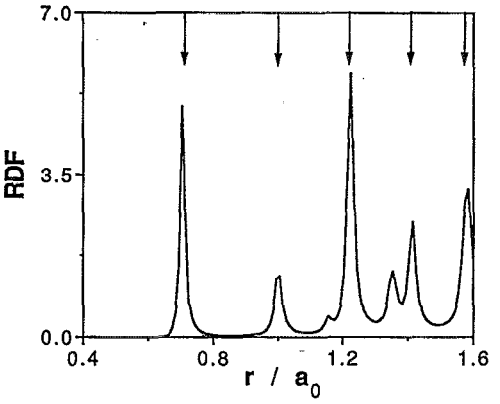

FIG. 11. The radial distribution function (RDF) for the polycrystal shows peaks close to the perfect-crystal positions (indicated by arrows) but broadened by the disorder at the grain boundaries and grain junctions.

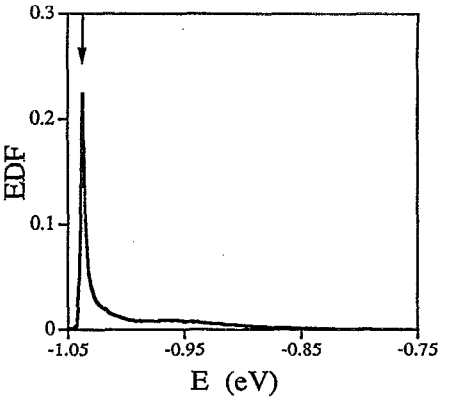

FIG. 12. The energy distribution function (EDF) for the polycrystal shows a sharp peak near the perfect-crystal cohesive energy (indicated by an arrow) and a broader higher-energy peak arising from the atoms at the grain boundaries and grain junctions.

0.11, 0.12, and 0.08 a_0 is obtained in the x, y, and z directions, respectively; this gives a mean value for the entire system of $\langle \delta V \rangle = 0.10\ a_0$.

The corresponding radial distribution function in Fig. 11 exhibits well-defined peaks characteristic of a well-ordered crystalline material. However, even at zero temperature these peaks are broadened by the presence of disorder due to the interfaces, and are slightly shifted from their perfect-crystal values (indicated by arrows). Interestingly, the maximum in the nn peak is at 0.7066 a_0 (i.e., shifted *downward* by 0.07% from its perfect-crystal position), indicating slightly compressed grain interiors and consistent with the stress contours in Figs. 10(a)–10(c). However, the mean nn peak position is shifted *upward* by 0.06% to 0.7075 a_0, in accordance with the lower density of the material. The contribution from second-nns does not have a single well-defined maximum, but instead exhibits three maxima of almost identical heights at 0.9986, 0.9994, and 1.0010 a_0. Also in accordance with the lower density, the mean position of this peak is shifted upward (by 0.3% to 1.0031 a_0).

The average nn miscoordination provides another useful tool for characterizing the average atomic structure. Using the definition of the miscoordination per unit GB area C in Eq. (2) and again assuming that all GBs are parallel to the faces of the simulation cell, an average value of $\langle C \rangle = 3.89\ a_0^{-2}$ is obtained. This value corresponds to each atom having 11.81 nn as defined by the area under the nn peak in Fig. 11 (i.e., out to the halfway point between the perfect-crystal first and second neighbors).

In analogy to the radial distribution function, we define an energy distribution function as the fractional number of atoms within a given small energy range. The energy distribution for the NCM shown in Fig. 12 exhibit a perfect-crystal peak at $E \approx -1.037$ eV and a higher-energy tail. Interestingly, this tail does not monotonically decrease in amplitude but, instead, exhibits a second, rather broad, peak at $E \approx -0.97$ eV attributable to the GBs and grain junctions. The excess energy of the system can be determined from this energy distribution, yielding an average GB energy, $\langle \gamma \rangle = 730$ erg/cm^2, again assuming that all GBs are parallel to the simulation-cell faces. This value would decrease slightly if the growth defects in the grain interiors were taken into account.

The above values for $\langle \delta V \rangle$, $\langle C \rangle$, and $\langle \gamma \rangle$ can be compared with related phase-space averaged values extracted from bicrystal studies. Lattice-statics simulation for bicrystals have shown that the GB energy γ, the miscoordination per unit area C, and the excess volume per unit GB area δV are intimately related.[12,20] Specifically, simulations of almost 300 different bicrystalline GBs in fcc metals (including symmetric and asymmetric, tilt, twist, general, high- and low-angle GBs) demonstrate an approximately linear relationship between the GB excess volume and the nn miscoordination per unit area, on the one hand, and the GB energy, on the other.[12,20] For the LJ potential used here, these simulations yield $\delta V = \alpha\gamma$, with $\alpha \approx 0.000143\ a_0$ cm^2/erg,[12] and $C = \beta\gamma$ with $\beta \approx 0.0075 a_0^{-2}$ cm^2/erg.[14,20] Insertion of the NCM value of $\langle \gamma \rangle = 730$ erg/cm^2 into the first expression yields $\langle \delta V \rangle = 0.10\ a_0$, in excellent agreement with the NCM value determined by MD; similarly, insertion into the second expression yields $\langle C \rangle = 5.49\ a_0^{-2}$; i.e., a somewhat larger miscoordination per unit GB area than the actual MD value ($3.9\ a_0^{-2}$), but still within the scatter of the bicrystal data.[14,20]

IV. PROPERTIES

Among the various properties that could be determined for our model NCM, here we only discuss the thermal expansion, the elastic behavior and the excess specific heat. While the investigation of the thermal expansion and the elastic properties addresses the issues of the isotropy of our model NCM, all three permit us to compare with the properties of coarse-grained materials.

A. Thermal expansion

As mentioned at the end of Sec. III B, our melt-grown model NCM is stable under thermal cycling at least up to 600 K, thereby providing information on the thermal expansion. Figure 13(a) shows the lattice expansion parallel to the three edges of the simulation cell (see Fig. 6) as a function of increasing temperature at 100 K intervals; as one would expect, the values on cooling were indistinguishable from those

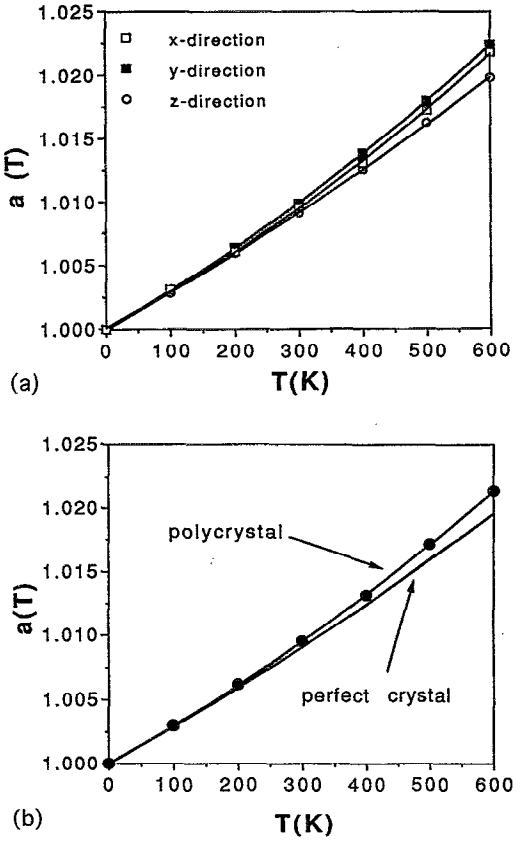

FIG. 13. (a) Temperature dependence of the anisotropic lattice parameters of the polycrystal in the x, y, and z directions (see Fig. 6) normalized to the zero-temperature value. (b) Mean normalized lattice parameter for the polycrystal compared with that of the perfect crystal.

obtained on heating. It is evident that there is a small anisotropy in the thermal expansion, with the expansion in the z direction being somewhat less than that in the x and y directions (see Fig. 6), which are very similar to each other.

Although the system is, therefore, not completely isotropic, we define a mean lattice parameter as the cube root of the volume of the system, i.e., as the geometrical mean of the simulation cell dimensions in the x, y, and z directions. Figure 13(b) compares the temperature dependence of this geometric-mean lattice parameter with the lattice parameter of the perfect crystal. Clearly, the polycrystal shows a small thermal-expansion enhancement above $T=300$ K, but is almost the same as the perfect crystal at lower temperatures, indicating that the thermal expansion of the GB regions is virtually indistinguishable from that of the bulk. This is consistent with the results of recent experiments on nanocrystalline Pd, which show no thermal-expansion enhancement below $T=300$ K.[7]

B. Elastic properties

Based on the reasonably isotropic density and thermal expansion, one would also expect a high degree of elastic isotropy. Here we investigate whether, in spite of consisting of only eight grains, our model polycrystal is indeed elastically isotropic, and compare the elastic moduli with those of the coarse-grained material.

As a benchmark against which to compare our results, we briefly discuss the elastic moduli of a coarse-grained polycrystalline material obtained from the elastic constants and moduli of the single crystal. As is the case for all equilibrium pair potentials, the LJ potential gives only two independent elastic constants; in the principal cubic ⟨100⟩ coordinates, they are $C_{11}=1.81\times10^{12}$ dyn/cm^2 and $C_{12}=C_{44}=1.02\times10^{12}$ dyn/cm^2 (10^{12} dyn/cm^2=0.1 TPa). The related single-crystal Young's bulk and shear moduli are $Y=1.08\times10^{12}$ dyn/cm^2, $B=1.28\times10^{12}$ dyn/cm^2 and $G=C_{44}=1.02\times10^{12}$ dyn/cm^2, respectively, with a Poisson ratio of $\nu=0.36$. The bulk modulus of a coarse-grained material with cubic symmetry is identical to that of the single crystal, i.e., $B^{\text{avg}}=1.28\times10^{12}$ dyn/cm^2.[27] The polycrystalline-averaged shear modulus can be calculated using a formalism due to Kröner[27] to be $G^{\text{avg}}=0.70\times10^{12}$ dyn/cm^2. The coarse-grained polycrystalline-averaged Young's modulus and Poisson ratio can then be calculated using the equations of continuum elasticity to be $Y^{\text{avg}}=1.78\times10^{12}$ dyn/cm^2 and $\nu^{\text{avg}}=0.27$.

The elastic constants of the polycrystal were calculated from stress–strain curves, produced by straining the polycrystal in the appropriate manner, allowing all the atomic forces to relax, and then calculating the resulting stresses on the system. The elastic moduli were then calculated from the full 6×6 elastic-constant tensor in the usual way.

While for an isotropic system the bulk modulus, B, is given by $B=(C_{11}+2C_{12})/3$, strictly speaking it is not even defined for a system which is not exactly isotropic. Nevertheless, we have calculated approximate values of the bulk modulus using various appropriate combinations of C_{11}, C_{22}, and C_{33} with $2C_{12}$, $2C_{13}$, and $2C_{23}$. All estimates obtained are in the range $1.14-1.21\times10^{12}$ dyn/cm^2, with a mean value of $B^{\text{poly}}=1.18\times10^{12}$ dyn/cm^2, which is 92% of the polycrystalline-average bulk modulus. For the Young's modulus in the x, y, and z directions (see Fig. 6) we obtained 1.29, 1.33, and 1.26×10^{12} dyn/cm^2, for a mean value of $Y^{\text{poly}}=1.29\times10^{12}$ dyn/cm^2, which is 73% of the Young's modulus of the coarse-grained material. The narrow range of values for the Young's and bulk moduli are indicative of a high degree of elastic isotropy of our model NCM. For the three shear moduli G, we obtain the values 0.39, 0.30, and 0.47×10^{12} dyn/cm^2 and the six Poisson ratios lie in the range 0.13–0.20. That the shear moduli are less isotropic than the Young's and bulk moduli is reasonable, since the values of the shear constants in bicrystalline multilayers are known to be much more sensitive to the atomic-level structure of the GBs.[28]

While experimentally determined elastic moduli of NCMs are generally lower than those of coarse-grained materials, due in part to pores and other structural flaws, it is hard to determine their intrinsic elastic response.[4,29] A direct comparison between the simulation results and experiment is therefore difficult, if not impossible.

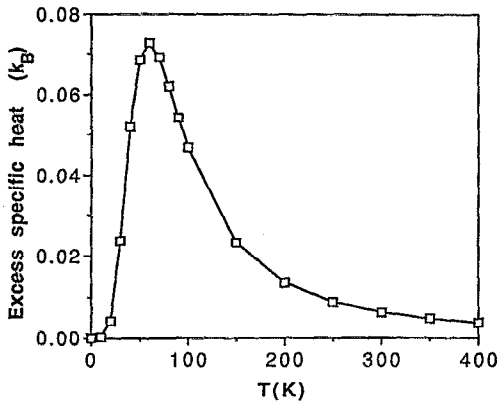

FIG. 14. Excess specific heat of the polycrystal shows a peak of height 0.075 k_B at $T \approx 60$ K.

C. Specific heat

Starting from the zero-temperature structure, we have used lattice-dynamics calculations to determine the phonon contribution to the low-temperature thermodynamic properties. Particularly striking is the appearance of a specific-heat anomaly discussed in the following.

Within the framework of lattice dynamics, phonon properties are usually determined in the harmonic approximation (HA). However, due to the large amounts of computer memory required in diagonalizing the $3N \times 3N$ dynamical matrix, the HA cannot be used for systems containing more than typically about 500 atoms. The so-called local-harmonic approximation used here, a computationally efficient and less computer-memory intensive approximation to the HA, is known to give reliable results for the thermodynamic properties of the perfect crystal and systems containing point defects.[30]

According to Fig. 14, the low-temperature excess specific heat thus obtained exhibits a pronounced peak at about 60 K, with a height of about 0.075 k_B (corresponding to an enhancement of 21% over the bulk value). A comparison with the excess specific heat of a simple monodisperse model of a NCM demonstrates that this peak is completely due to the interfacial disorder in the system, which gives rise to a low-frequency tail in the phonon density of states.[31] Also, the appearance of such a peak is in qualitative agreement with the experimental results.[32,33] It has been suggested that these anomalies may be due either to increased anharmonicity at the GBs or to the presence of light-element impurities.[32] While we cannot rule out any additional effects due to impurities, the results demonstrate that an anomaly can arise from phonon effects alone.

V. DISCUSSION

Extensive studies of mechanical properties of polycrystalline materials by Rosenhain and others during the first half of this century[34] led to the widely held view of the "amorphous-cement" nature of GBs.[35] However, mostly based on observations in bicrystals and coarse-grained polycrystals of (a) good long-range structural periodicity of the GBs, (b) well-defined rigid-body translations, and (c) a large variation of the GB energy with misorientation, *the model* has been discredited. For the highly constrained GBs in NCMs, however, the model assumptions appear to be much better satisfied, as evidenced by the absence of strict translational periodicity parallel to the GBs and a relatively uniform GB thickness and energy.

Consistent with Rosenhain's historic GB model,[34] the previously discussed results suggest that the detailed atomic structures of the GBs may not be of great importance to the properties of these highly constrained systems. Instead, the most important structural feature of NCMs appears to lie in the existence of heavily disordered structural inhomogeneities of more or less uniform width which act as a "cement-like" phase holding the grains together. Such a simple two-phase structural model is supported by local-probe types of experiments, such as Mössbauer spectroscopy,[8] which clearly demonstrate the existence of a GB phase that is distinct from the bulk, perfect-crystal-like phase. The structure and properties of this disordered "NCM cement" may be characterized, for example, by its average width, reduced density, and increased energy density. However, the question as to whether this disordered GB phase is actually amorphous is not easily resolved because, due to its severe confinement, one cannot reasonably expect its properties to resemble those of a *bulk* glass. An analogous situation exists in the tribology area, where it is well known that the structures and properties of thin, confined liquid layers can differ dramatically from those of bulk liquids.

VI. CONCLUSIONS

As pointed out in the Introduction, at present it appears that experimental investigations alone may not be capable of deriving a comprehensive structural model for nanocrystalline materials or of establishing the relationship of the structures of the highly constrained GBs in these materials with those well known from bicrystal studies. In this first simulation study of its kind, our goal has been to demonstrate that atomistic computer simulations can, indeed, provide insights into these questions not otherwise obtainable.

While we have not attempted to address any of the kinetics-related issues at the heart of the experimental difficulties in reproducibly synthesizing fully dense NCMs, here we have aimed at a thermodynamics-based description of what we consider a "relaxed, metastable ground state" towards which these materials should ultimately evolve. We hope to have demonstrated that the MD synthesis of a space-filling, fully dense NCM by crystallization from the melt provides a rather direct route towards such a state. Our method is similar to the experimental synthesis of NCMs by crystallization of amorphous materials, a method also known to produce highly dense NCMs free of voids. In addition, our simulation method permits the grain-size distribution and the types of GBs in the system to be carefully controlled and, hence, to be correlated with the simulated properties of the material.

Although in our first application of this method only eight grains were included in the simulation cell, the resulting material exhibits nevertheless a reasonably isotropic density, thermal expansion, and elastic moduli. Surprisingly, the

density and thermal expansion differ relatively little from those in the perfect crystal; the elastic moduli, however, are somewhat lower than in the coarse-grained material. Apart from a phonon-induced anomaly in the excess specific heat, our model material, therefore, behaves rather normally, in spite of its small grain size. This observation suggests that reports of highly anomalous properties of NCMs were obtained either for highly "unrelaxed" states of the GBs in these materials[11] or that the effects were controlled by the porosity or impurities in the material.

In spite of rather "normal" properties, the structures of the GBs in our NCM differ fundamentally from those well known from bicrystal studies. The ability in our simulations to control the misorientations between the grains has enabled us to compare some of the GB structures in the NCM directly with those of the corresponding bicrystalline GBs. This comparison has demonstrated that:

(a) In the highly inhomogeneous NCM, regions of considerably lower density (at the GBs and grain junctions) coexist with regions of slightly higher density (in the grain interiors), as evidenced by the positions and widths of the peaks in the radial distribution function.

(b) Due to the severe microstructural constraints in the NCM, the rigid-body translations parallel to the GBs cannot be optimized simultaneously for all the GBs in the system, as illustrated most strikingly for the (111) coherent twin boundary. Giving rise to the coexistence of short, high-energy GB facets with different rigid-body translations, this effect apparently destroys the long-range periodicity commonly observed in bicrystalline GBs.

(c) The severely constrained environment in NCMs gives rise to an increase in the energies of low-energy bicrystalline GBs; by contrast, GBs with an already very high energy in the bicrystal have similar energies in the NCM because their energies cannot be increased further, even by the microstructural constraints. Based on these two effects, one can expect a much narrower distribution of the GB energies in the NCM than in bicrystals.

(d) Although still highly localized, the GBs in our 43 Å grain-sized NCM are wider (typically by about 50%) than in bicrystals; however, for the same reason as for the energies, the distribution in these widths is rather narrow.

(e) Apart from an important role played by the microstructural constraints, the absence of strict structural periodicity parallel to the GBs in both MD-grown bicrystal and in the NCM suggests the existence of relaxations (e.g., GB reconstruction) that do not exist in bicrystals produced by lattice-statics relaxation. Such additional relaxations may be associated with the high atom diffusivity in the liquid and give rise to reconstructions with an associated GB densification particularly of those GBs with a very high energy in the bulk-terminated bicrystal.

(f) In conclusion, the considerably greater degree of isotropy of key GB parameters and the absence of strict long-range structural periodicity parallel to the GBs suggests a simple structural model for NCMs in which, in zeroth order, the GBs are viewed as an isotropic, cement-like phase with a more or less uniform width, density, excess-energy density, and miscoordination per unit volume. Although the structure and excess-energy density of this GB phase are neither bulk-glass-like nor can they be described in terms of structural models and parameters derived from bicrystal studies, the concept of a cement-like phase connecting the nanometer-sized grains, reminiscent of Rosenhain's "amorphous-cement" model,[34,35] describes our observations rather well.

ACKNOWLEDGMENTS

The authors have benefited from discussions with Dr. W. Hahn (Saarbrücken), Dr. J. A. Eastman, and Dr. J. Wang (ANL). S.R.P. and D.W. were supported by the US Department of Energy, BES-Materials Science under Contract No. W-31-109-Eng-38.

[1] H. Gleiter, in *Proceedings of the Second Risø International Symposium on Metallurgy and Materials Science*, edited by N. Hansen, A. Horsewell, T. Leffers, and H. Lilholt (Risø National Laboratory, Roskilde, Denmark, 1981), p. 15.
[2] R. Birringer, H. Gleiter, H.-P. Klein, and P. Marquardt, Phys. Lett. A **102**, 365 (1984).
[3] X. Zhu, R. Birringer, U. Herr, and H. Gleiter, Phys. Rev. B **35**, 9085 (1987).
[4] H. Gleiter, Prog. Mater. Sci. **33**, 223 (1989).
[5] C. A. Melendres, A. Narayanasamy, V. A. Maroni, and R. W. Siegel, J. Mater. Res. **4**, 1246 (1989).
[6] G. J. Thomas, R. W. Siegel, and J. A. Eastman, Scr. Metall. Mater. **24**, 201 (1990).
[7] J. A. Eastman, M. R. Fitzsimmons, and L. J. Thompson, Philos. Mag. B **66**, 667 (1992).
[8] J. Jiang, S. Ramasamy, R. Birringer, U. Gonser, and H. Gleiter, Solid State Commun. **80**, 525 (1991); U. Herr, J. Jing, R. Birringer, U. Gonser, and H. Gleiter, Appl. Phys. Lett. **50**, 472 (1987).
[9] V. Y. Gertsman, R. Birringer, R. Z. Valiev, and H. Gleiter, Scr. Metall. Mater. **30**, 229 (1994).
[10] W. Wunderlich, Y. Ishida, and R. Maurer, Scr. Metall. **24**, 403 (1990).
[11] J. Löffler, J. Weissmüller, and H. Gleiter, *Proceedings of the Second International Conference on Nanostructured Materials, Stuttgart, 1994*, edited by H. Gleiter, H.-E. Schaefer, and T. Tsakalakos (Pergamon, New York, 1995), in press; and submitted to Phys. Rev. B.
[12] D. Wolf, Scr. Metall. **23**, 1913 (1989).
[13] K. L. Merkle, Ultramicroscopy **40**, 281 (1992); Interface Sci. (in press); K. L. Merkle and M. I. Buckett, in *Proceedings of the 52nd Annual Meeting of the Microscopy Society of America*, edited by G. W. Bailey and A. J. Garratt-Reed (Electron Microscopy Society of America, San Francisco, 1994), p. 722.
[14] D. Wolf, J. Appl. Phys. **68**, 3221 (1990).
[15] D. Wolf and J. F. Lutsko, Phys. Rev. Lett. **60**, 1170 (1988).
[16] M. P. Anderson, G. S. Grest, and D. J. Srolovitz, Philos. Mag. B **59**, 293 (1989).
[17] H. Gleiter, in Ref. 11.
[18] D. Wolf, J. Phys. Coll. C **4**, 197 (1984).
[19] M. P. Allen and D. J. Tildesley, *Computer Simulation of Liquids* (Clarendon, Oxford, 1987).
[20] See, for example, D. Wolf and K. L. Merkle, in *Materials Interfaces: Atomic-Level Structure and Properties*, edited by D. Wolf and S. Yip (Chapman and Hall, London, 1992), p. 87.
[21] D. Wolf and J. F. Lutsko, J. Mater. Res. **4**, 1427 (1989).
[22] D. Wolf and J. Jaszczak, J. Comp.-Aided Mat. Design **1**, 111 (1993).
[23] S. R. Phillpot, J. Appl. Phys. **72**, 5606 (1992).
[24] S. R. Phillpot, J. Mater. Res. **9**, 582 (1994).
[25] D. G. Brandon, B. Ralph, S. Ranganathan, and M. S. Wald, Acta Metall. **12**, 813 (1964); B. Chalmers and H. Gleiter, Philos. Mag. **23**, 1541 (1971).
[26] M. Weins, H. Gleiter, and B. Chalmers, Scr. Metall. **4**, 732 (1970); J. Appl. Phys. **42**, 2639 (1971); D. A. Smith, V. Vitek, and R. C. Pond, Acta Metall. **25**, 475 (1977).
[27] E. Kröner, J. Eng. Mech. Div. **5**, 889 (1980).

[28] D. Wolf and M. D. Kluge, Scr. Metall. **24**, 907 (1990).
[29] R. W. Siegel and G. E. Fougere, in *Nanophase Materials*, edited by G. C. Hadjipanayis and R. W. Siegel (Kluwer, Dordrecht, 1994), p. 233.
[30] R. LeSar, R. Najafabadi, and D. J. Srolovitz, J. Chem. Phys. **94**, 5090 (1991).
[31] J. Wang, D. Wolf, S. R. Phillpot, and H. Gleiter (unpublished).
[32] A. Tschöpe and R. Birringer, Philos. Mag. B **68**, 223 (1993).
[33] H. G. Klein, Diplom thesis, Universität des Saarlandes, 1992.
[34] W. Rosenhain and J. C. W. Humfrey, J. Iron Steel Inst. **87**, 219 (1913); W. Rosenhain and D. Ewen, J. Inst. Met. **10**, 119 (1913).
[35] For an excellent review, see K. T. Aust and B. Chalmers, in *Metal Interfaces* (ASM, Cleveland, 1952), p. 153.